RSC Advances

PAPER

View Article Online
View Journal | View Issue

Cite this: *RSC Adv.*, 2023, **13**, 29721

Intrinsic half-metallicity in two-dimensional Cr_2TeX_2 (X = I, Br, Cl) monolayers†

Jun Zhang,[a] Zixin He,[a] Chuchu Gao,[a] Yanyan Tao,[a] Feng Liang,[a] Guannan Li,[a] Benling Gao *[a] and Guang Song *[ab]

Received 24th August 2023
Accepted 27th September 2023

DOI: 10.1039/d3ra05780a

rsc.li/rsc-advances

Two-dimensional (2D) materials with intrinsic half-metallicity at or above room temperature are important in spin nanodevices. Nevertheless, such 2D materials in experiment are still rarely realized. In this work, a new family of 2D Cr_2TeX_2 (X = I, Br, Cl) monolayers has been predicted using first-principles calculations. The monolayer is made of five atomic sublayers with ABCAB-type stacking along the perpendicular direction. It is found that the energies for all the ferromagnetic (FM) half-metallic states are the lowest. The phonon spectrum calculations and molecular dynamics simulations both demonstrate that the FM states are stable, indicating the possibility of experimentally obtaining the 2D Cr_2TeX_2 monolayers with half-metallicity. The Curie temperatures from Monte Carlo simulations are 486, 445, and 451 K for Cr_2TeI_2, Cr_2TeBr_2, and Cr_2TeCl_2 monolayers, respectively, and their half-metallic bandgaps are 1.72, 1.86 and 1.90 eV. The corresponding magnetocrystalline anisotropy energies (MAEs) are about 1185, 502, 899 μeV per Cr atom for Cr_2TeX_2 monolayers, in which the easy axes are along the plane for the Cr_2TeBr_2 and Cr_2TeCl_2 monolayers, but being out of the plane in the Cr_2TeI_2. Our study implies the potential application of the 2D Cr_2TeX_2 (X = I, Br, Cl) monolayers in spin nanodevices.

I. Introduction

The discovery of graphene in 2004 has greatly promoted the research upsurge on two-dimensional (2D) materials because of their prominent advantages in electronics, magnetism, spintronics, optoelectronics, batteries and sensors due to the quantum confinement effect.[1–8] In spintronic nanodevices, the 2D ferromagnetic (FM) materials with half-metallicity, are desired as perfect candidates for producing full spin polarization, injection, and transport.[2,9] However, most of the pristine 2D materials are short of magnetism, and the inevitable inhomogeneity of magnetism obtained by doping, defecting, edging, *etc.*, is disadvantageous to spintronics, so it is very necessary to obtain pristine 2D materials with the intrinsic magnetism.[10–13]

It is known that obtaining the 2D materials with intrinsic magnetism is difficult because the magnetic order of the 2D isotropic Heisenberg model at finite temperatures is forbidden according to the Mermin–Wagner (M–W) theorem.[14] The 2D anisotropic crystals can effectively overcome the limitation of M–W principle. The 2D CrI_3 and $Cr_2Ge_2Te_6$ with the FM structure obtained experimentally in recent years are the outstanding progress of the long-range FM ordering in atomic thin materials.[15,16] However, their Curie temperatures (T_C) of 45 and 20 K are too low, which obviously confines the applications in practice.

Accordingly, it is particularly urgent to search for the 2D FM materials with high Curie temperatures. Through continuous-unremitting and arduous efforts, in recent years, some 2D materials with high T_C have been realized theoretically or experimentally, whose values are far exceeding the liquid-nitrogen transition temperature and even reaching room temperature.[17–26] These are extremely important progress. However, among these high T_C 2D FM materials, some are semiconductors,[17–21] while others are normal FM metals rather than FM half-metals.[22–26]

Considering the practical applications in spintronics, it is perfect for a 2D FM half-metal to have wide half-metal bandgaps and large magnetocrystalline anisotropy energy (MAE) besides possessing the high T_C. That is to say, the 2D FM half-metals with three distinguishing features: high T_C, wide half-metal bandgaps, and sizeable MAEs, are essentially pursued for the realization of the practical spintronic devices. So far, many 2D intrinsic half-metals have been proposed, such as 2D $CoGa_2X_4$ (X = S, Se, or Te),[27] Mn_2CF_2 MXene,[28] Cr_3X_4 (X = S, Se, Te),[29] Co_2O_3,[30] Fe_2CF_2,[31] Fe_4N_2 pentagon crystal,[32] Cr_2C,[33] Janus monolayer V_2XN (X = P, As),[34] *etc.*, but the vast majority of these materials only have some of the three factors and few can fully meet all these requirements. Therefore, exploring new 2D half-metallic materials with higher Curie temperatures, wider half-metallic bandgaps, and larger MAEs has always been a very important and meaningful work.

[a]*Department of Physics, Huaiyin Institute of Technology, 1 Meicheng East Road, Huaian 223003, China. E-mail: jsblgao@163.com; gsong@hyit.edu.cn*

[b]*Department of Physics, Nanjing University, 22 Hankou Road, Nanjing 210093, China*

† Electronic supplementary information (ESI) available. See DOI: https://doi.org/10.1039/d3ra05780a

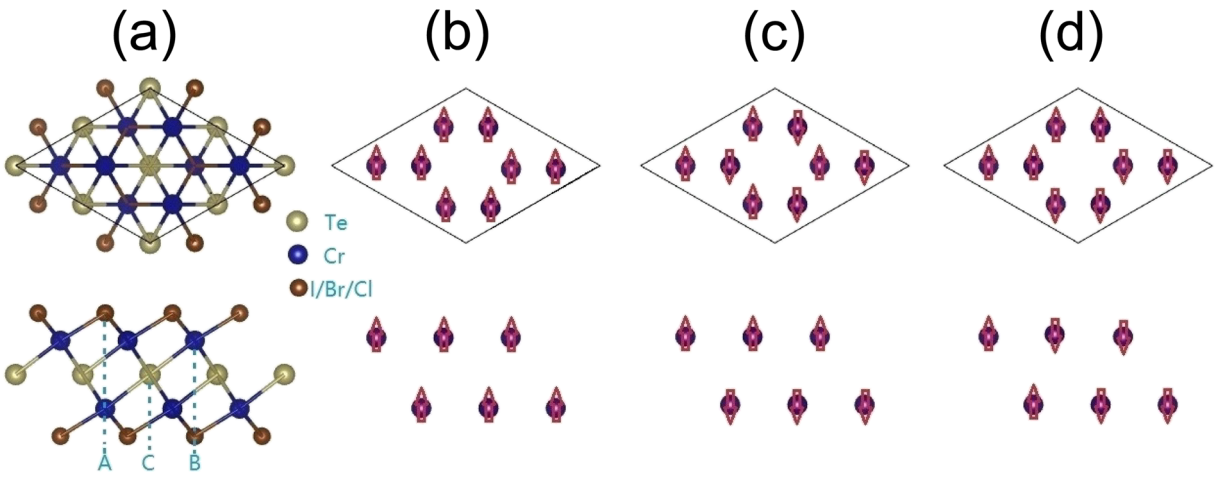

Fig. 1 Geometric and magnetic configurations of Cr_2TeX_2 monolayers from top (above) and side (below) views: (a) structures of 2 × 2 × 1 supercell, (b) FM, (c) AFM-1, and (d) AFM-2.

In this paper, we propose a new family of 2D Cr_2TeX_2 (X = I, Br, Cl) monolayers. It is composed of five trigonal atomic sublayers X_1–Cr_1–Te–Cr_2–X_2 with ABCAB-type stacking along the *z*-direction (*c*-axis), shown as Fig. 1(a). Two antiferromagnetic (AFM) configurations besides the FM (as Fig. 1(b)) are named as AFM-1 and AFM-2 (as Fig. 1(c) and (d)), in which AFM-1 means that the intra- and inter-sublayers are FM and AFM, respectively, but in AFM-2, the intra-sublayers are AFM, and the magnetic states in two Cr-sublayers are same. The lowest energy states are found to be FM half-metal. In the Cr_2TeX_2 monolayers, the Curie temperature and the direction of the magnetization easy axis are related to the type of halogen atoms. Our Monte Carlo simulations based on the classic Heisenberg model show that the Curie temperatures are about 486, 445, and 451 K for Cr_2TeI_2, Cr_2TeBr_2, and Cr_2TeCl_2 monolayers, respectively. The large MAEs show their potential applications in magnetic memory and storage, in which the easy axe directions are along the plane for the Cr_2TeBr_2 and Cr_2TeCl_2 monolayers, but is out of plane in Cr_2TeI_2. Besides, they also have considerable half-metal bandgaps. These properties make the 2D Cr_2TeX_2 (X = I, Br, Cl) monolayers have good potential application in spin nanodevices.

II. Method and computational details

Our calculations based on the first-principles of density functional theory (DFT) are carried out by using the VASP code.[35,36] The projector augmented wave method is adopted for describing the ion–electron interaction and the plane-wave cutoff energy is set to be 550 eV. The Brillouin-zone integration is sampled on a 21 × 21 × 1 Monkhorst–Pack *k*-point mesh grid for geometry optimization.[37] The generalized gradient approximation (GGA) in the version of Perdew–Burke–Ernzerhof (PBE) is used for the electron exchange and correlation.[38,39] For the structural optimization of different magnetic states, a collinear initial magnetic moment configuration is adopted as shown in Fig. 1, and when calculating the MAE of the FM state, the spin–orbit coupling (SOC) effect is considered. The effective on-site interaction U_{eff} = 2.0 eV is used to describe the Hubbard correction, and the selection of the U_{eff} is mainly based on the consideration that in similar structures in many other works, such values on Cr atoms can make the calculation results better approximate or agree with the experiment.[40–42]

The periodic boundary conditions are adopted and a vacuum layer of 25 Å in the non-periodic *c*-axis direction is used to eliminate the interactions between the periodic images. The energy convergence is set to 10^{-7} eV for the electron relaxation and the structure optimization is stopped until the force acting on each atom is less than 0.005 eV $Å^{-1}$. Dynamic stabilities and phonon dispersion curves are obtained using the phonopy code based on the density functional perturbation theory (DFPT).[43] *Ab initio* molecular dynamics (AIMD) simulations are used to check the thermal stability of the structures using a Nosé–Hoover thermostat.[44] In all the molecular dynamics simulations, the time step is 1 fs and the total time lasts for 10 ps. In order to estimate the Curie temperature, Monte Carlo (MC) simulations are implemented based on the Heisenberg model of 40 × 40 × 1 supercell.

III. Results and discussions

The Cr_2TeX_2 monolayers possess the geometric structure with a D_{3d} symmetry ($P3m1$) space group, as shown in Fig. 1(a). Each Cr atom is connected to three X and three Te atoms, and each X atom is connected to three Cr atoms, while each Te atom is coordinated with six Cr atoms. To study the preferred coupling of magnetic moments in Cr_2TeX_2 monolayers, we consider three typical magnetic coupling configurations in a 2 × 2 × 1 supercell. Three spin configurations include one FM coupling and two AFM couplings shown in Fig. 1(b) and (c), which are called AFM-1 and AFM-2, respectively. The Cr atoms in the two adjacent rows from top (above) view in Fig. 1 correspond to two different Cr sublayers, indicating two different *c*-axis coordinates. Table 1 shows the relative energies between the FM and AFMs. Among all monolayers, the FM state has the lowest energy, meaning that the Cr_2TeX_2 monolayers have a FM

Table 1 Relative energies of the different magnetic configurations per 2 × 2 × 1 supercell. The energy of FM state is taken as zero. J_1 and J_2 represent the intra-sublayer and inter-sublayer exchange parameters, respectively

	FM, meV	AFM1, meV	AFM2, meV	E_{coh}, eV	MAE1, μeV	MAE2, μeV	J_1, meV	J_2, meV
Cr_2TeI_2	0.0	2359.2	1963.1	2.660	1185	1191	9.193	24.575
Cr_2TeBr_2	0.0	2506.3	1701.9	2.898	−502	−490	6.770	26.107
Cr_2TeCl_2	0.0	2516.7	1728.8	3.114	−899	−888	6.952	26.216

Table 2 Optimized lattice parameters of the FM ground states. *a* and *b* represent the lattice constants, d_{Cr} and d_X correspond to the distances between the two Cr and two X sublayers, respectively. ℓ_{X-Cr} and ℓ_{Cr-Te} represent the nearest distances between X and Cr atoms, and between Cr and Te atoms, respectively. The lengths are in units of Å

Categories	$a(=b)$	d_{Cr}	d_X	ℓ_{X-Cr}	ℓ_{Cr-Te}
Cr_2TeI_2	4.128	3.352	6.528	2.864	2.914
Cr_2TeBr_2	3.965	3.480	6.294	2.687	2.876
Cr_2TeCl_2	3.866	3.561	6.053	2.556	2.855

ground state. The total magnetic moments are about $8\mu_B$ for the FM states, showing large spin polarizations in the 2D Cr_2TeX_2 monolayers.

The optimized structure parameters of the FM ground states are summarized in Table 2 for the unit cell of Cr_2TeX_2 monolayers. One can see that the lattice constant (a, b) and thickness (d_X) of Cr_2TeX_2 monolayers increase with the radius of halogen atom increasing, while the distance (d_{Cr}) between the two planes of Cr atoms decreases. This is because the interactions of the bigger halogen atoms with the Cr atoms are weaker, which leads to more stronger attraction of Cr to Te atoms.

In order to investigate the relative stability of the 2D Cr_2TeX_2 (X = I, Br, Cl) monolayers, we calculate the cohesive energy defined as $E_{coh} = (2E_{Cr} + 2E_X + E_{Te} - E_{Cr_2TeX_2})/5$ with E_{Cr}, E_X, E_{Te} and $E_{Cr_2TeX_2}$ being the energies of a single atom of Cr, X, Te, and of one unit of $E_{Cr_2TeX_2}$ monolayer, respectively. The obtained cohesive energies of the Cr_2TeX_2 (X = I, Br, Cl) monolayers are 2.66, 2.90, and 3.11 eV per atom for the FM states, respectively, which are comparable to those of V_3X_8 (X = I, Br, Cl) monolayers (2.92, 3.38, and 3.84 eV per atom),[45] indicating that the Cr_2TeX_2 monolayers should be stable.

To demonstrate the dynamical stabilities of the Cr_2TeX_2 (X = I, Br, Cl) monolayers, we calculate their phonon spectra. From the results shown in Fig. 2, one can see that there exist no negative vibrational frequencies in the phonon dispersions, confirming that the three structures with the FM states are stable for all monolayers. The thermal stabilities of these FM monolayers are also investigated by AIMD simulations. In the simulations, a 5 × 5 × 1 supercell containing 125 atoms is considered. At the temperature of 300 K, the Nosé–Hoover temperature and energy changes with time are shown in Fig. 3, in which the two physical quantities vary with time always around a stable value. Moreover, it can be seen from the top-side views that there is no chemical bond fracture and structural reconstruction after 10 ps. This implies that the three FM monolayers are thermally stable.

To further understand the magnetism of the FM ground states, the spin-resolved band structures have been calculated and plotted in Fig. 4. It can be seen that the spin-up states are all metallic, while the spin-down ones exhibit semiconductor characteristics. The energy gaps of the spin-down states from Fig. 4(b), (d) and (f) are 2.50, 2.49, and 2.37 eV for the Cr_2TeI_2, Cr_2TeBr_2, and Cr_2TeCl_2 monolayers, respectively, showing the indirect bandgaps between the Γ point of the valence band top and the M point of the conduction band bottom. Compared with the spin-down ones, the spin-up states are occupied by more electrons below the Fermi energy. There are two bands crossing the Fermi energy twice, which are mainly contributed by the orbitals of Cr-e_g and X-p from Fig. 5, making half of the two bands below the Fermi energy. Together with the extra seven full bands, the occupied number of the spin-up states is about 8 more than that of the spin-down ones below the Fermi level, thus resulting in the magnetic moment of about $8.0\mu_B$ per cell. As the SOC may open a bandgap and make metals transform into semiconductors, in order to verify the rigidity of half-

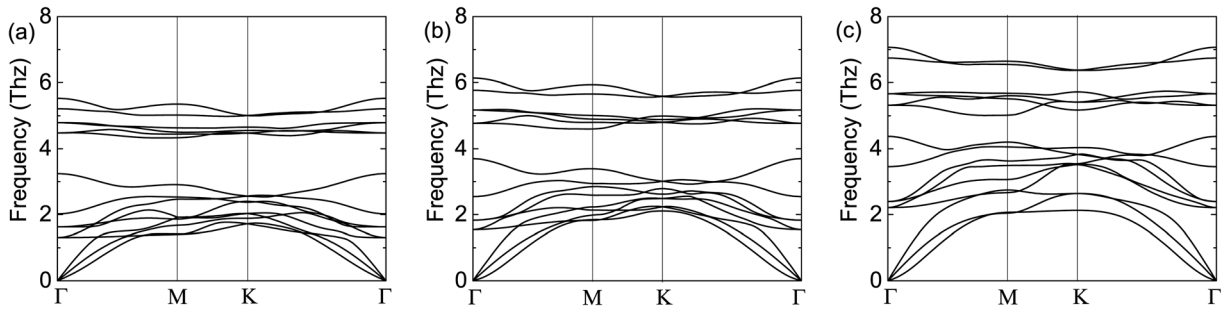

Fig. 2 Calculated phonon spectra of the FM states: (a) for Cr_2TeI_2, (b) for Cr_2TeBr_2, and (c) for Cr_2TeCl_2. In the calculation, the expansion of 3 × 3 × 1 for the primitive cell Cr_2TeX_2 is adopted.

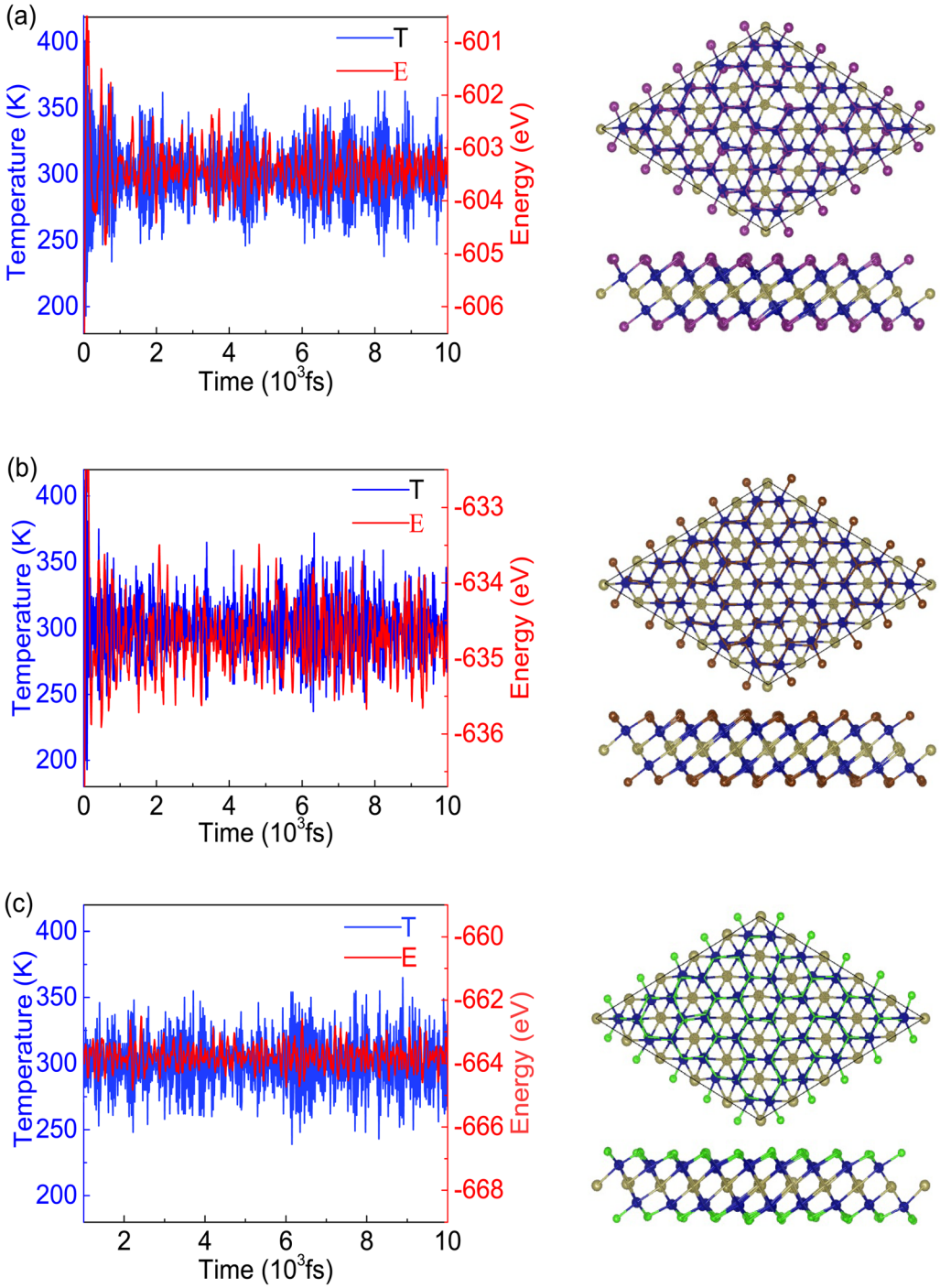

Fig. 3 The time evolution of the temperature (K) and the corresponding energy (eV) (left), and the top-side views (right) after 10 ps simulation at 300 K for the three systems: (a) Cr_2TeI_2, (b) Cr_2TeBr_2, and (c) Cr_2TeCl_2 monolayers obtained from the AIMD simulations of 125 atoms.

metallic properties, we have also calculated the band structure considering SOC, and the results show that there are several energy bands passing through the Fermi level, indicating the reliability of the half-metallicity of the Cr_2TeX_2 monolayers (see Fig. S1 in ESI†).

In order to determine the stability of the half-metallicity, we calculate the half-metallic bandgap, which is defined as the energy gap from the Fermi level to the conduction band minimum in spin-down channel and represents the preventing ability that a electron at Fermi level flips its spin from the spin-up channel to the spin-down one. The half-metallic bandgaps are 1.72, 1.86, and 1.90 eV for the Cr_2TeI_2, Cr_2TeBr_2 and Cr_2TeCl_2 monolayers, being comparable to those (1.55, 1.94, and 1.78 eV) of Mn_2X_3 (X = Te, Se, S) monolayers[46] and 1.53 eV of YN_2 monolayer,[47] and such large values mean that half-metallic properties have high stability and 100% spin polarization can

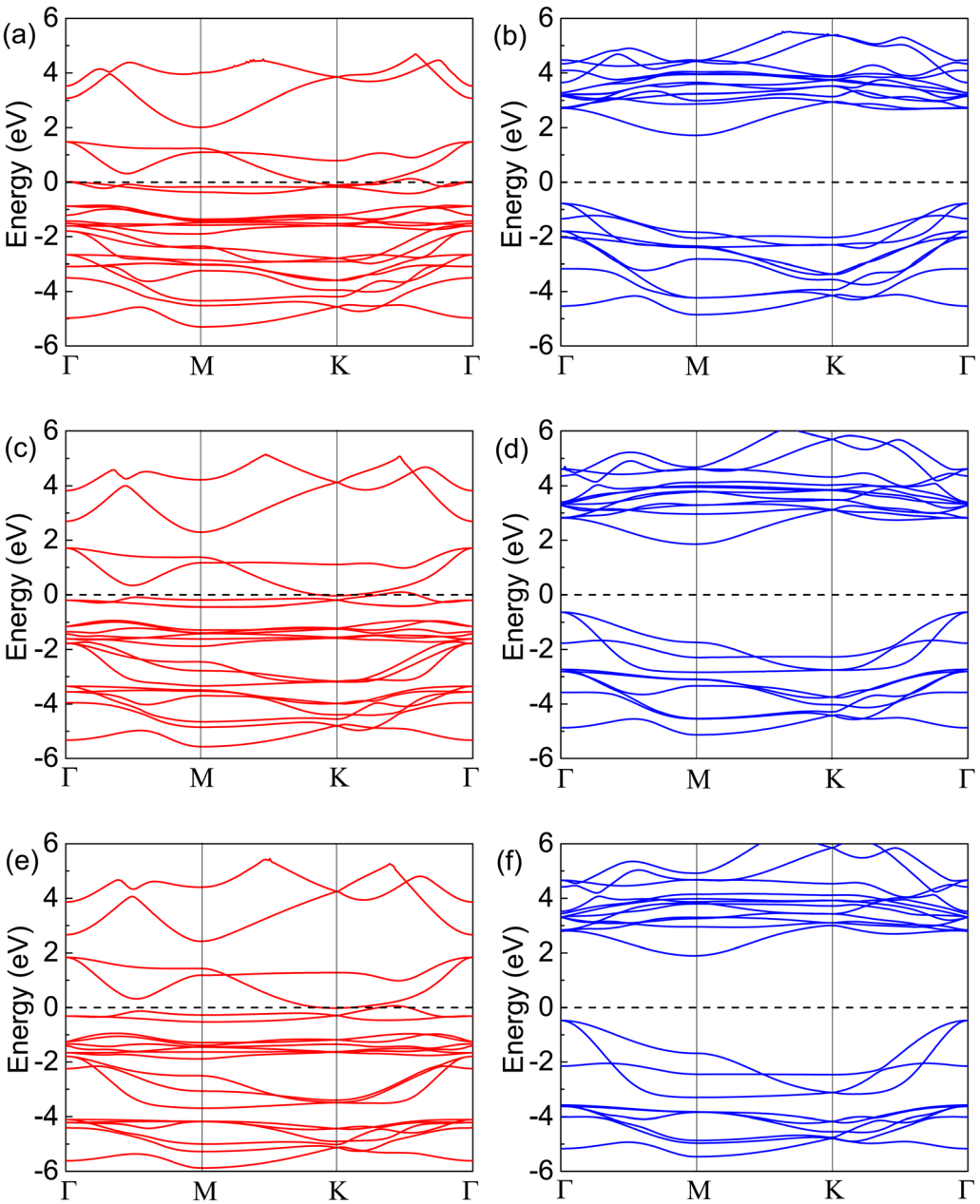

Fig. 4 Calculated band structures of Cr_2TeX_2 monolayers with spin-up (left: marked in red color) and spin-down (right: marked in blue color) channels: (a) and (b) for Cr_2TeI_2, (c) and (d) for Cr_2TeBr_2, (e) and (f) for Cr_2TeCl_2. The dashed-black line at zero eV denotes the Fermi energy E_f. The coordinates of the high symmetry points are Γ = (0, 0, 0), M = (0.5, 0, 0) and K = (1/3, 1/3, 0).

be easily maintained. In order to verify the reliability of the half-metallicity of the three monolayers, we have also conducted a calculation with $U_{eff} = 3.0$ eV. The results show that all ground states of the three monolayers are still ferromagnetic under U_{eff} = 3.0 eV, and all band structures (see Fig. S2 in ESI†) also exhibit half-metallicity with wide half-metallic bandgaps (2.08, 2.27, and 2.33 eV for the Cr_2TeI_2, Cr_2TeBr_2, and Cr_2TeCl_2 monolayers, respectively). This indicates that the characteristic of the FM half-metallicity with wide half-metallic bandgaps do not change with the changes of U_{eff}.

In order to further explain the FM ground states, the specific orbital densities of states of the Cr, Te and X atoms are calculated and shown in Fig. 5. The maximum contribution to the states near the Fermi level is from the d-orbitals of Cr atoms. In the Cr_2TeX_2 monolayers, each Cr atom forms octahedral coordination with three Te atoms and three X ligands, which causes the Cr-d orbitals to split into two parts: the t_{2g} (d_{xy}, d_{xz}, and d_{yz}) and e_g (d_{z^2} and $d_{x^2-y^2}$) manifolds. Each Cr atom can provide two electrons on its outer orbitals to form bonds with X and Te atoms. Meanwhile, the remaining four electrons are divided into two parts, in which three electrons half occupy the lower t_{2g} orbitals and one will half occupy the higher e_g orbitals and lead to a magnetic moment of about $4\mu_B$ per Cr atom (see Fig. 5). It is seen that the angles ($\theta_{Cr-Te-Cr}$ and $\theta_{Cr-X-Cr}$) Cr–Te–Cr

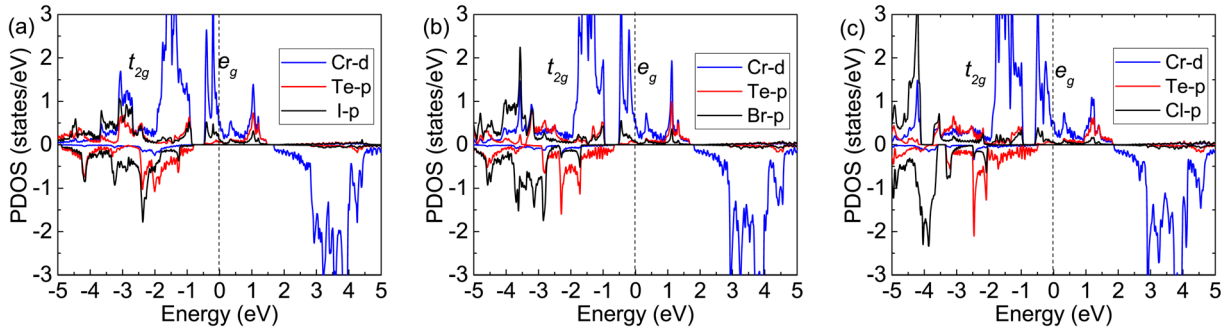

Fig. 5 Calculated partial density of states with FM: (a) for Cr_2TeI_2, (b) for Cr_2TeBr_2, and (c) for Cr_2TeCl_2. The dashed-black line at zero eV denotes the Fermi energy E_f.

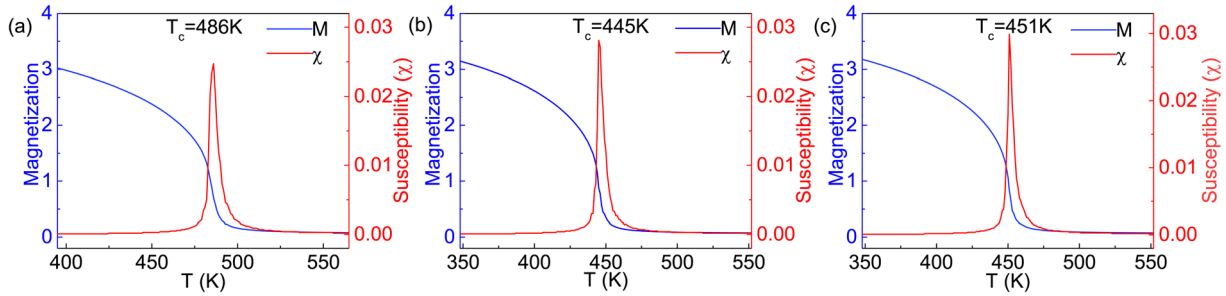

Fig. 6 Average magnetic moment and susceptibility of the primitive Cr_2TeX_2 monolayer as a function of temperature, obtained from the Monte Carlo simulations with the 2D Heisenberg model: (a) Cr_2TeI_2, (b) Cr_2TeBr_2, and (c) Cr_2TeCl_2.

and Cr–X–Cr in the three monolayers are all close to 90° from the results of the structural optimizations. Based on the Goodenough–Kanamori–Anderson (GKA) rules,[48–50] the electronic configuration is helpful to the formation of FM exchange between the nearest-neighbor (NN) Cr atoms. On the other hand, the half-occupied e_g orbitals pass through the Fermi energy, resulting in the emergence of half-metallicity.

The Curie temperature T_C is an important physical parameter for the constituent materials of spintronic devices, because the magnetism can only be maintained at temperatures below T_C. In order to overcome the drawback of overestimating the Curie temperature by mean field method and obtain a more accurate value of T_C, we carry out the MC simulations with the MC code based on the 2D Heisenberg model,[51] $H = -\sum_{i,j} J_{ij} S_i S_j - \sum_i D_i S_{iz}^2$, in which S is the magnetic moment of a single Cr atoms, J_{ij} is the exchange parameter between the i-th and j-th Cr atoms, and D is the magnetic anisotropy parameter. The sum of i, j in the formula includes the nearest neighbors in the intra- and inter-sublayer, and the corresponding exchange parameters are denoted as J_1 and J_2, respectively. To calculate J_1 and J_2, we choose the relative energies of the FM and the above AFM-1 and AFM-2 orders, and make use of the following equations,

$$E_{FM} = E_0 - (24J_1 + 12J_2)S^2, \quad (1)$$

$$E_{AFM\text{-}1} = E_0 - (24J_1 - 12J_2)S^2, \quad (2)$$

$$E_{AFM\text{-}2} = E_0 - (-8J_1 + 4J_2)S^2. \quad (3)$$

The obtained parameters of J_1 and J_2 are listed in Table 1. It can be seen from the J_1 and J_2 values that the intralayer coupling is obvious weaker than the interlayer one, similar to the case of 2D Cr_2C monolayers,[52] in which the next-nearest-neighbor coupling is stronger than the nearest-neighbor one. Due to the fact that in the same Cr sublayer, a Cr atom has six nearest-neighbor Cr atoms, while a Cr atom has three nearest-neighbor Cr atoms between two Cr sublayers, the contribution of J_1 to the Curie temperature will be significantly greater than that of J_2 if the changes of J_1 and J_2 are similar. In our simulations, the spins on arbitral Cr atoms can flip freely in positive or negative directions. The magnetic moment and susceptibility of the 2D supercell at equilibrium under each given temperature are calculated, as shown in Fig. 6. The estimated values of T_C are about 486, 445, and 451 K for the Cr_2TeI_2, Cr_2TeBr_2, and Cr_2TeCl_2 monolayers, respectively, which are considerably higher than the room temperature of 300 K. Due to the different spin directions of the three monolayers, we have also calculated the relative energies of the three magnetic states with SOC, and then obtained the exchange parameters J_1 and J_2 (see Table S1 in ESI†). From the parameters, we have performed the MC simulations again, and the obtained values of T_C with SOC are 475, 438, and 445 K for the Cr_2TeI_2, Cr_2TeBr_2, and Cr_2TeCl_2 monolayers, respectively (see Fig. S3 in ESI†). This indicates that the Curie temperature remains basically unchanged when considering the spin direction, showing that the results of the FM transition temperature above room temperature are reliable, and

implying that the Cr_2TeX_2 (X = I, Br, Cl) monolayers may have the application probability in practice.

Finally, let's calculate the magnetocrystalline anisotropy energy (MAE), defined as MAE1/2 = $E(100)/(010) - E(001)$, which is a signature of ability for the magnetic order to resist thermal disturbances and also is an important parameter related to the thermal stability of magnetic information storage. A large MAE mean storing more information, which is more conducive to device miniaturization. The calculated MAE1/2 are 1185/1191, −502/−490, and −899/−888 μeV per Cr atom for Cr_2TeI_2, Cr_2TeBr_2, and Cr_2TeCl_2 FM states, respectively, which are significantly higher than those of some previously reported monolayers such as $CrBr_3$ (186 μeV per Cr),[17] CrOBr (290 μeV per Cr),[18] CrSBr (146 μeV per Cr),[19] Cr_3Te_4 (150 μeV per Cr),[29] *etc.*, and also have comparability with those of the $InCrTe_3$ (1442 μeV per Cr)[21] and Cr_2O_3 (900 μeV per Cr)[30] monolayers. The differences between MAE1 and MAE2 are 6, 12, and 11 μeV per Cr atom for Cr_2TeI_2, Cr_2TeBr_2, and Cr_2TeCl_2 FM states, respectively, showing in-plane magnetic crystal anisotropy. Due to the tiny difference, the effect on Curie temperature and magnetic susceptibility can be ignored. As one can see, the MAE value of the Cr_2TeI_2 in the three monolayers is the biggest because the I atom is the heaviest and its SOC strength is much stronger than those of the other atoms. It is particularly noted that the easy axe (magnetization direction) is out of the plane for the Cr_2TeI_2 monolayer, and the direction along the out-of-plane is better to the storage and adjustment of information, while the axes are in plane for the Cr_2TeBr_2 and Cr_2TeCl_2 monolayers. However, although the Br atom is heaver than the Cl one, the MAE of the Cr_2TeBr_2 is smaller than that of the Cr_2TeCl_2. This can be explained by the MAE formula from the second-order perturbation theory,[53,54] and it can be expressed as, $\mathrm{MAE1/2} = \sum_{o,u}(\left|H_{ou}^{SOC}(\vec{x}/\vec{y})\right|^2 - \left|H_{ou}^{SOC}(\vec{z})\right|^2)/(E_u - E_o)$, here E_u (E_o) is the energy of occupied (nonoccupied) state o (u), and $H_{ou}^{SOC}(\vec{n}) = \xi\langle\psi_o|\vec{\sigma}\cdot\vec{L}|\psi_u\rangle$ is the SOC matrix element, in which ξ is the SOC strength, are Pauli matrics, and $\vec{L}$ is the orbital angular momentum operator. It can be seen that the MAE is not only related to the size of transition-matrix elements between two states, but also to the energy differences in between. Although the SOC in the Cr_2TeBr_2 may be stronger than that in the Cr_2TeCl_2, it is possible that the MAE in the Cr_2TeBr_2 monolayer is smaller than that in the Cr_2TeCl_2. And the similar phenomena also occur in other structures, such as the GdX_2 and GdX (X = Cl, Br) monolayers, in which the MAEs of the $GdCl_2$ and GdCl monolayers are bigger than those of the $GdBr_2$ and GdBr ones.[55,56] The large out-of-plane MAE makes the Cr_2TeI_2 monolayer possessing potential applications in high-density information storage.

IV. Summary

By performing first-principles DFT calculations, we have predicted that the 2D Cr_2TeX_2 (X = I, Br, Cl) monolayers with ABCAB-type stacking along the perpendicular direction are FM half-metals. The structures are dynamically stable. The Curie temperatures are all above room temperature, as obtained from the Monte Carlo simulations based on the Heisenberg model. Especially, they possess wide half-metallic bandgaps and sizeable MAEs, and the magnetization direction of the Cr_2TeI_2 monolayer is out of plane, showing their potential application value in spin nanodevices and information storages. Our study implies that the 2D Cr_2TeX_2 (X = I, Br, Cl) monolayers may have the potential application in realizing spin nanodevices.

Conflicts of interest

The authors have no conflicts of interest to disclose.

Acknowledgements

This work was supported by the National Natural Science Foundation of China under Grant No. 11774296 and 11974296.

References

1 K. S. Novoselov, A. K. Geim, S. V. Morozov, D. Jiang, Y. Zhang, S. V. Dubonos, I. V. Grigorieva and A. A. Firsov, *Science*, 2004, **306**, 666.
2 S. A. Wolf, D. D. Awschalom, R. A. Buhrman, J. M. Daughton, S. von Molnár, M. L. Roukes, A. Y. Chtchelkanova and D. M. Treger, *Science*, 2001, **294**, 1488.
3 Z. Guo, S. Chen, Z. Wang, Z. Yang, F. Liu, Y. Xu, J. Wang, Y. Yi, H. Zhang and L. Liao, *Adv. Mater.*, 2017, **29**, 1703811.
4 X. Yang, X. Zhang, J. Deng, Z. Chu, Q. Jiang, J. Meng, P. Wang, L. Zhang, Z. Yin and J. You, *Nat. Commun.*, 2018, **9**, 570.
5 R. Wang, X. Li, Z. Wang and H. Zhang, *Nano Energy*, 2017, **34**, 131.
6 Y. Zhang, B. Zheng, C. F. Zhu, X. Zhang, C. L. Tan, H. Li, B. Chen, J. Yang, J. Z. Chen, Y. Huang, L. H. Wang and H. Zhang, *Adv. Mater.*, 2015, **27**, 935.
7 S. Q. Zhang, R. Z. Xu, N. N. Luo and X. L. Zou, *Nanoscale*, 2021, **13**, 1398.
8 X. Jiang, Q. X. Liu, J. P. Xing, N. S. Liu, Z. F. Liu and J. J. Zhao, *Appl. Phys. Rev.*, 2021, **8**, 031305.
9 N. Miao and Z. Sun, *Wiley Interdiscip. Rev.: Comput. Mol. Sci.*, 2021, **12**, e1545.
10 S. Jiang, L. Li, Z. Wang, K. F. Mak and J. Shan, *Nat. Nanotechnol.*, 2018, **13**, 549.
11 R. R. Nair, M. Sepioni, I. L. Tsai, O. Lehtinen, J. Keinonen, A. V. Krasheninnikov, T. Thomson, A. K. Geim and I. V. Grigorieva, *Nat. Phys.*, 2012, **8**, 199.
12 S. Dutta, A. K. Mann and S. K. Pati, *Phys. Rev. Lett.*, 2009, **102**, 096601.
13 X. Hong, K. Zou, B. Wang, S. H. Cheng and J. Zhu, *Phys. Rev. Lett.*, 2012, **108**, 226602.
14 N. D. Mermin and H. Wagner, *Phys. Rev. Lett.*, 1966, **17**, 1133.
15 B. Huang, G. Clark, E. Navarro-Moratalla, D. R. Klein, R. Cheng, K. L. Seyler, D. Zhong, E. Schmidgall, M. A. McGuire, D. H. Cobden, W. Yao, D. Xiao, P. Jarillo-Herrero and X. D. Xu, *Nature*, 2017, **546**, 270.
16 C. Gong, L. Li, Z. L. Li, H. W. Ji, A. Stern, Y. Xia, T. Cao, W. Bao, C. Z. Wang, Y. Wang, Z. Q. Qiu, R. J. Cava, S. G. Louie, J. Xia and X. Zhang, *Nature*, 2017, **546**, 265.

17 W. B. Zhang, Q. Qu, P. Zhu and C. H. Lam, *J. Mater. Chem. C*, 2015, **3**, 12457.
18 N. Miao, B. Xu, L. Zhu, J. Zhou and Z. Sun, *J. Am. Chem. Soc.*, 2018, **140**, 2417.
19 H. Wang, J. S. Qi and X. F. Qian, *Appl. Phys. Lett.*, 2020, **117**, 083102.
20 N. Sivadas, M. W. Daniels, R. H. Swendsen, S. Okamoto and D. Xiao, *Phys. Rev. B: Condens. Matter Mater. Phys.*, 2015, **91**, 235425.
21 G. Song, D. S. Li, H. F. Zhou, C. F. Zhang, Z. W. Li, G. N. Li, B. W. Zhang, X. K. Huang and B. L. Gao, *Appl. Phys. Lett.*, 2021, **118**, 123102.
22 X. Jiang, Q. X. Liu, J. P. Xing and J. J. Zhao, *J. Phys. Chem. Lett.*, 2019, **10**, 7753.
23 Z. Fei, B. Huang, P. Malinowski, W. Wang, T. Song, J. Sanchez, W. Yao, D. Xiao, X. Zhu, A. F. May, W. Wu, D. H. Cobden, J. H. Chu and X. Xu, *Nat. Mater.*, 2018, **17**, 778.
24 Y. Deng, Y. Yu, Y. Song, J. Zhang, N. Z. Wang, Z. Sun, Y. Yi, Y. Z. Wu, S. Wu, J. Zhu, J. Wang, X. H. Chen and Y. B. Zhang, *Nature*, 2018, **563**, 94.
25 H. Wang, Y. Liu, P. Wu, W. Hou, Y. Jiang, X. Li, C. Pandey, D. Chen, Q. Yang, H. Wang, D. Wei, N. Lei, W. Kang, L. Wen, T. X. Nie, W. S. Zhao and K. L. Wang, *ACS Nano*, 2020, **14**, 10045.
26 Y. J. Niu, K. Zhang, X. F. Cui, X. J. Wu and J. L. Yang, *Nano Lett.*, 2023, **23**, 2332.
27 S. Q. Zhang, R. Z. Xu, W. H. Duan and X. L. Zou, *Adv. Funct. Mater.*, 2019, **29**, 1808380.
28 J. J. He, P. Lyu and P. Nachtigall, *J. Mater. Chem. C*, 2016, **4**, 11143.
29 X. Zhang, B. Wang, Y. Guo, Y. Zhang, Y. Chen and J. Wang, *Nanoscale Horiz.*, 2019, **4**, 859.
30 A. Hashmi, K. Nakanishi, M. U. Farooq and T. Ono, *npj 2D Mater. Appl.*, 2020, **4**, 39.
31 Y. Hu, X. Y. Liu, Z. H. Shen, Z. F. Luo, Z. G. Chen and X. L. Fan, *Nanoscale*, 2020, **12**, 11627.
32 K. Zhang, M. L. Chen, D. Y. Wang, H. F. Lv, X. J. Wu and J. L. Yang, *Nanoscale*, 2021, **13**, 19493.
33 S. Das, A. Kabiraj and S. Mahapatra, *Nanoscale*, 2022, **14**, 9409.
34 W. Wan, B. T. Fu, C. Liu, Y. F. Gea and Y. Liu, *Phys. Chem. Chem. Phys.*, 2023, **25**, 9311.
35 G. Kresse and J. Hafner, *Phys. Rev. B: Condens. Matter Mater. Phys.*, 1993, **48**, 13115.
36 G. Kresse and J. Furthmüller, *Comput. Mater. Sci.*, 1996, **6**, 15.
37 H. J. Monkhorst and J. D. Pack, *Phys. Rev. B: Solid State*, 1976, **13**, 5188.
38 P. E. Blöchl, *Phys. Rev. B: Condens. Matter Mater. Phys.*, 1994, **50**, 17953.
39 G. Kresse and D. Joubert, *Phys. Rev. B: Condens. Matter Mater. Phys.*, 1999, **59**, 1758.
40 J. L. Lado and J. Fernández-Rossier, *2D Mater.*, 2017, **4**, 035002.
41 C. X. Huang, J. S. Feng, F. Wu, D. Ahmed, B. Huang, H. J. Xiang, K. M. Deng and E. J. Kan, *J. Am. Chem. Soc.*, 2018, **140**, 11519.
42 X. B. Lu, R. X. Fei and L. Yang, *Phys. Rev. B*, 2019, **100**, 205409.
43 A. Togo, F. Oba and I. Tanaka, *Phys. Rev. B: Condens. Matter Mater. Phys.*, 2008, **78**, 134106.
44 G. J. Martyna, M. L. Klein and M. Tuckerman, *J. Chem. Phys.*, 1992, **97**, 2635.
45 H. B. Xiao, X. N. Wang, R. L. Wang, L. F. Xu, S. H. Liang and C. P. Yang, *Phys. Chem. Chem. Phys.*, 2019, **21**, 11731.
46 C. J. Yu, X. Y. Li, X. X. Li and J. L. Yang, *J. Phys. Chem. Lett.*, 2021, **12**, 11790.
47 Z. F. Liu, J. Y. Liu and J. J. Zhao, *Nano Res.*, 2017, **10**, 1972.
48 P. W. Anderson, *Phys. Rev.*, 1950, **79**, 350.
49 J. B. Goodenough, *Phys. Rev.*, 1955, **100**, 564.
50 J. Kanamori, *J. Phys. Chem. Solids*, 1959, **10**, 87.
51 L. Liu, X. Ren, J. Xie, B. Cheng, W. Liu, T. An, H. Qin and J. Hu, *Appl. Surf. Sci.*, 2019, **480**, 300.
52 C. Si, J. Zhou and Z. M. Sun, *ACS Appl. Mater. Interfaces*, 2015, **7**, 17510.
53 D. S. Wang, R. Q. Wu and A. J. Freeman, *Phys. Rev. B: Condens. Matter Mater. Phys.*, 1993, **47**, 14932.
54 G. H. O. Daalderop, P. J. Kelly and M. F. H. Schuurmans, *Phys. Rev. B: Condens. Matter Mater. Phys.*, 1994, **50**, 9989.
55 S. J. Li, W. Jiang, Y. F. Hou, F. W. Zheng, X. H. Shao and P. Zhang, *J. Appl. Phys.*, 2021, **130**, 043902.
56 Y. W. Wang, X. C. Zhang, Z. H. Gao, T. F. Cao, J. Q. Shi and X. L. Fan, *J. Phys. Chem. C*, 2023, **127**, 4643.